THE ASTROPHYSICAL JOURNAL, 162:947–962, December 1970

ON THE UPPER MASS LIMIT FOR MAIN-SEQUENCE STARS

KENNETH ZIEBARTH*
Joint Institute for Laboratory Astrophysics, University of Colorado, Boulder
Received 1970 April 27; revised 1970 July 27

ABSTRACT

Two aspects of the problem of the upper mass limit are investigated. First, a linear nonadiabatic analysis is used to investigate the dependence of this limit on composition. Second, a nonlinear hydrodynamic calculation has been carried out to study the consequences for a star whose mass exceeds the limit. The maximum stable mass is not found to be a sensitive function of composition. This mass, $\mathfrak{M}_c$, decreases with increasing Y at fixed Z; at fixed Y, $\mathfrak{M}_c$ decreases with decreasing Z. In the hydrodynamic calculation it was necessary to increase artificially the very slow growth rate of the pulsations. After initiation of small-amplitude pulsations in the fundamental mode, the pulsations grew to a limiting amplitude too small to produce mass loss. It is shown that the artificial increase in growth rate probably greatly underestimates the shock-wave dissipation. If this is true, mass loss may never occur. Instead, stars with masses above the stability limit may simply pulsate at some (perhaps small) amplitude until nuclear evolution stabilizes them.

I. INTRODUCTION

As was first pointed out by Ledoux (1941), the dominance of radiation pressure over gas pressure results in an upper mass limit to pulsationally stable, chemically homogeneous stars. This limit is a result of the fact that as Γ_1 approaches $\frac{4}{3}$ (the value for isotropic blackbody radiation), pulsations become nearly homologous. Hence pulsation amplitudes have finite values even in the stellar core. These amplitudes allow the destabilizing effect of nuclear reactions to compete with the stabilizing effect of radiative transfer in the envelope, so that for large enough masses, pulsational instability is possible. The value of this mass limit found by Ledoux (1941) was approximately $100\,\mathfrak{M}_\odot$. Subsequent investigation by Schwarzschild and Härm (1959) found a value of $60\,\mathfrak{M}_\odot$. In addition, Stothers and Simon (1970) have recently investigated the effects of opacity on this mass limit. The first goal of the present investigation is an independent study of the dependence of this mass limit on composition.

It has been assumed previously that a star whose mass exceeds the stability limit will pulsate with ever increasing amplitude until mass is ejected from the surface and a stable mass is reached. This mass loss must occur in a rather short time since nuclear evolution is a strong stabilizing mechanism. It was shown by Schwarzschild and Härm (1959) and confirmed by Stothers and Simon (1968) that as soon as a significant fraction of the hydrogen in the core is converted to helium, the stars become very stable. Since the time scale for this nuclear evolution is short at such large masses, stars near but above the mass limit may be stabilized before mass loss occurs. The second part of this paper describes a hydrodynamic calculation of the pulsational evolution of a star whose mass is above the mass limit. The goal is a test of the mass-loss hypothesis.

The results, summarized previously (Ziebarth 1970), indicate that the upper mass limit for stable stars is not a sensitive function of composition. This mass, $\mathfrak{M}_c$, decreases with increasing Y at fixed Z. For fixed Y, $\mathfrak{M}_c$ decreases slowly with decreasing Z. The mass-loss prediction was not confirmed by the hydrodynamic calculation. A limiting amplitude was reached before mass loss occurred and before effects of nuclear evolution could become important. This limiting amplitude was reached in spite of the fact that shock-wave dissipation was greatly underestimated. It seems probable that this dissipa-

* Present address: Department of Physics, University of Calgary, Calgary 44, Alberta, Canada.

tion will limit the amplitude of the pulsations until stabilization caused by nuclear evolution can become effective.

II. COMPUTATIONAL METHODS

a) Static and Dynamic Calculations

Whenever possible, standard computational techniques for stellar structure and stability have been used. Stellar models in hydrostatic and thermal equilibrium representing the main sequence near and above the expected stability limit were constructed. The method used was a Newton-Raphson technique similar in principle to that first applied by Henyey *et al.* (1959) and used later in various forms by many others. Each of these models was then analyzed for pulsational stability by using a linear nonadiabatic program described in the next section. The dynamic evolution of one model (100.1) found to be unstable was followed in detail. The method used for this calculation was based on that of Cox, Brownlee, and Eilers (1966).

The partial differential equations which describe the structure and motion of spherically symmetric stars are the following:

$$\frac{\partial r}{\partial \mathfrak{M}_r} = \frac{1}{4\pi r^2 \rho}, \tag{1}$$

$$\frac{\partial^2 r}{\partial t^2} = -4\pi r^2 \frac{\partial P}{\partial \mathfrak{M}_r} - \frac{G\mathfrak{M}_r}{r^2}, \tag{2}$$

and

$$\frac{\partial E}{\partial t} + P\frac{\partial V}{\partial t} = \epsilon - \frac{\partial L_r}{\partial \mathfrak{M}_r}, \tag{3}$$

where standard notation is used throughout. A fourth equation describes the flow of energy through the star. This equation will be represented here only by the functional form

$$L_r = f[\rho(r), T(r)]\,. \tag{4}$$

The exact form of equation (4) depends, of course, on the means of energy transport. In this investigation radiation and conduction are treated by the standard diffusion method. Convection is treated in the static models by the mixing-length theory as described in chapter 14 of Cox and Giuli (1968). In practice this simply requires that the temperature gradient in the convective cores be adiabatic. In the linear analysis and in the dynamics it is assumed that, since convective lifetimes are much longer than the pulsation period, the convective luminosity is constant in time at its equilibrium value. Although this assumption is not completely correct, the effects of convection on stability have been previously investigated by Boury, Gabriel, and Ledoux (1964). Their results showed that the effect of holding the convective luminosity constant is only a change of a few percent in the stability.

In addition to these equations, one must specify certain gas characteristic relations and boundary conditions. In this investigation the following methods were used. In all calculations complete ionization was assumed, so the equation of state included only perfect-gas and blackbody radiation. Opacity was computed by interpolation in a table based on data from Cox and Stewart (1965) and modified by Paczyński (1969) to include Compton scattering and conduction. Nuclear energy generation was assumed to come exclusively from the CNO bi-cycle. An explicit formula based on reaction rates given by Fowler, Caughlan, and Zimmerman (1967) was used. Phase delays in energy generation were neglected. The surface boundary condition was placed at the photosphere and required that the gas pressure be zero but that the radiation pressure be the one associated with the effective temperature.

b) Linear Nonadiabatic Analysis

The pulsational stability of each of the models was investigated by using a linear nonadiabatic code written by Castor (1970). This code was originally designed for study of stellar envelopes and was modified to include nuclear generation of energy so that entire stellar models could be investigated.

The code solves a set of linearized complex difference equations for a complex eigenfrequency ω. This solution is obtained iteratively by using as a first approximation the adiabatic period and a quasi-adiabatic growth rate. In all cases the nonadiabatic period was found to differ negligibly from the adiabatic period. The nonadiabatic growth rate differed by at most a few percent from the quasi-adiabatic value.

c) The Amplification Factor

The growth rate of pulsations for these stars is always much longer than the period. For example, in the model for which dynamic evolution was calculated, the e-folding time for change of pulsational energy was approximately 10^6 periods. Clearly, the use of ordinary methods to follow dynamic evolution far enough to study the energy growth is economically impossible. For this reason an artificial technique for increasing the growth rate was used. This technique makes use of the fact that periods are determined by the time dependence of the momentum-conservation equation (2) whereas the growth rate is determined by the nonadiabatic terms in the energy-conservation equation (3). Since these two time scales are almost totally decoupled for our models, we can change the growth rate with almost no effect on the period. This change will be effected if we simply increase the nonadiabatic terms in the energy equation by some artificial amplification factor F. This equation then becomes

$$\frac{\partial E}{\partial t} + P\frac{\partial V}{\partial t} = F\left(\epsilon - \frac{\partial L_r}{\partial \mathfrak{M}_r}\right). \tag{5}$$

Two other interpretations of this amplification factor are helpful in understanding its effect. First, it is clear that in the difference form of the energy equation, F will simply multiply the time step Δt. Thus for every Δt by which we advance the changes in momentum, we advance the energy changes by $F\Delta t$. Second, it is possible by using thermodynamic identities to rewrite equation (5) as

$$\frac{\partial \ln T}{\partial t} = (\Gamma_3 - 1)\frac{\partial \ln \rho}{\partial t} + \frac{1}{c_v T}\left[F\left(\epsilon - \frac{\partial L_r}{\partial \mathfrak{M}_r}\right)\right]. \tag{6}$$

In this form we can see that we have effectively reduced the specific heat c_v by the factor F. Thus, since the heat capacity of the material is reduced, more energy can appear as work.

If the effect of the amplification factor were linear, we should expect that the relative energy gain per period would be increased by the factor F. Thus if we want to decrease the e-folding time so that computing times become reasonable, say to a value equal to the period, we must use an F of approximately 10^6. The actual effect is, of course, not linear in F, so that in practice $F \approx 4 \times 10^5$ is large enough to increase the growth rate by a factor 10^6.

The effects of such a large amplification factor on the physics of the problem are of course also large. These effects have been studied by using the linear nonadiabatic method described above; they will be discussed in § III. It is clear that with such a large amplification factor, the best possible result will be a qualitative understanding of large-amplitude pulsations driven by nuclear energy.

This method of increasing the growth rate of pulsations has been independently suggested by Talbot (1970). He has made several numerical experiments on the effects of

the method on small-amplitude nonlinear calculations and finds that the method gives a valid approximation for these small amplitudes in agreement with our conclusions.

A different method has been suggested by Appenzeller (1970). This method involves multiplying all velocities by a factor slightly larger than unity at the end of each time step. This has the disadvantage of introducing higher harmonics which decay very slowly. Thus a special differencing method is necessary to damp these harmonics. Although this method is no more artificial than the amplification-factor method, we feel that the problem of harmonics makes it somewhat less satisfactory.

III. RESULTS

a) The Static Models

The first part of this investigation consisted of computing a grid of homogeneous stellar models in hydrostatic and thermal equilibrium. These models represent the upper end of the main sequence and have masses ranging from 60 to 110 $\mathfrak{M}_\odot$. At each mass, models were constructed with six different compositions. These are variants of the Aller Population I composition (Aller 1961) and are shown in Table 1. The numbering of compositions reflects only the order in which computations were made. The ratio of

TABLE 1

COMPOSITIONS USED IN STABILITY ANALYSIS

Composition #1:*	Composition #3:	Composition #5:
X =0.59603	X =0.49603	X =0 57603
Y =0 38388	Y =0.48388	Y =0 38388
Z =0.02009	Z =0 02009	Z =0 04009
X_{CNO}=0 01219	X_{CNO}=0.01219	X_{CNO}=0 02433
Composition #2:	**Composition #4:**	**Composition #6:**
X =0 69603	X =0 79603	X =0.60603
Y =0 28388	Y =0 18388	Y =0 38388
Z =0 02009	Z =0 02009	Z =0.01009
X_{CNO}=0 01219	X_{CNO}=0 01219	X_{CNO}=0 00612

* Aller I mix

the mass abundance of the CNO elements to Z was held fixed at the value from the Aller I composition, approximately 0.6. Each model is identified by a number $M.c$, where M is the mass in solar units and c is the composition number. Thus for example, Model 80.4 has mass 80 $\mathfrak{M}_\odot$ and composition number 4.

The main features of the models are listed in Table 2. More detailed properties which will be of interest in the discussion of stability are shown in Tables 3 and 4. As expected, the models form a continuation of the upper end of the main sequence in the Hertzsprung-Russell diagram. The main sequences for different compositions are nearly parallel. The mass-luminosity relations for all compositions are nearly linear, as simple arguments predict.

All of the models are qualitatively similar to one another in their internal structure. For this reason a quantitative description will be given for only one case, Model 100.1 (the model for which dynamic evolution was calculated). In Figure 1 we show the relative masses, radii, and luminosities, and the density as a function of the zoning used. Note in particular that the outer 20 percent of the radius contains less than 1 percent of the mass. The convective core contains approximately 80 percent of the stellar mass, and convection carries at least half of the luminosity through 25 percent of the radius.

The ratio of gas pressure to total pressure, β, is approximately 0.5 at the center, as shown in Table 2. It then increases as one moves outward to lower temperatures. Since the surface boundary condition requires that the pressure be purely radiative, i.e., $\beta = 0$, there is a steep drop in β in the outer few percent of the mass. Since Γ_1 is a

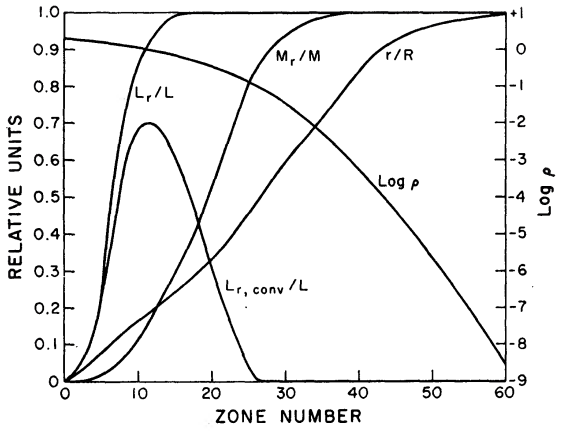

FIG. 1.—Mass, radius, luminosity, and density distributions of a typical static model (100.1)

Table 2

Main Properties of the Static Models

Model	$R/10^{11}$ (cm)	$L/10^{39}$ (erg/sec)	T_e (°K)	M_{bol}	$T_c/10^7$ (°K)	$P_c/10^{16}$ (dyne/cm^2)	V_c (cm^3/gm)	β_c
60.1	7.31	2.58	51013	- 9.83	4.05	1.67	.502	.593
70.1	7.96	3.39	52340	-10.13	4.11	1.64	.547	.562
80.1	8.55	4.26	53470	-10.38	4.16	1.62	.588	.536
90.1	9.12	5.18	54366	-10.59	4.20	1.61	.625	.513
100.1	9.67	6.13	55067	-10.77	4.23	1.60	.660	.493
110.1	10.19	7.12	55690	-10.93	4.26	1.59	.694	.475
60.2	7.28	2.13	48727	- 9.62	3.96	1.66	.507	.626
70.2	7.90	2.83	50188	- 9.93	4.02	1.62	.554	.595
80.2	8.51	3.60	51387	-10.19	4.07	1.60	.597	.568
90.2	9.08	4.40	52307	-10.41	4.11	1.58	.637	.544
100.2	9.61	5.25	53140	-10.60	4.15	1.57	.674	.524
110.2	10.13	6.13	53803	-10.77	4.18	1.56	.708	.505
60.3	7.35	3.12	53350	-10.04	4.15	1.70	.494	.558
70.3	7.99	4.05	54617	-10.32	4.21	1.68	.536	.528
80.3	8.61	5.04	55571	-10.56	4.26	1.66	.575	.502
90.3	9.18	6.08	56402	-10.76	4.29	1.65	.611	.480
100.3	9.72	7.14	57060	-10.94	4.33	1.64	.644	.461
110.3	10.24	8.25	57638	-11.09	4.36	1.64	.675	.444
60.4	7.24	1.75	46519	- 9.41	3.88	1.66	.510	.657
70.4	7.88	2.37	48102	- 9.74	3.94	1.62	.559	.625
80.4	8.47	3.03	49336	-10.01	3.99	1.59	.604	.598
90.4	9.04	3.74	50336	-10.23	4.03	1.56	.645	.574
100.4	9.57	4.49	51209	-10.43	4.07	1.55	.683	.553
110.4	10.08	5.27	51936	-10.61	4.10	1.53	.719	.534
60.5	7.87	2.63	49402	- 9.85	3.91	1.42	.565	.585
70.5	8.57	3.46	50702	-10.15	3.97	1.40	.615	.554
80.5	9.22	4.34	51731	-10.40	4.01	1.38	.661	.528
90.5	9.82	5.27	52619	-10.61	4.05	1.37	.704	.505
100.5	10.41	6.24	53311	-10.79	4.08	1.36	.743	.486
110.5	10.98	7.24	53874	-10.95	4.11	1.36	.780	.468
60.6	6.90	2.54	52303	- 9.81	4.21	1.96	.446	.597
70.6	7.51	3.35	53726	-10.11	4.27	1.93	.486	.566
80.6	8.07	4.20	54843	-10.36	4.32	1.90	.522	.540
90.6	8.62	5.11	55731	-10.57	4.36	1.89	.556	.517
100.6	9.13	6.05	56487	-10.76	4.40	1.87	.587	.497
110.6	9.61	7.02	57143	-10.92	4.43	1.86	.616	.479

Table 3

Properties Affecting Stability (Z = .02009, fixed)

Model	Y	$\Gamma_{1,c}$	$\varepsilon_c/10^5$	κ_c	κ_s	<s>	$\rho_c/<\rho>$
			(erg/gm sec)	(cm^2/gm)	(cm^2/gm)		
60.4	.18388	1.464	3.48	.323	.759	.127	26.12
60.2	.28388	1.456	4.18	.304	.677	.119	26.71
60.1	.38388	1.447	5.00	.286	.604	.112	27.31
60.3	.48388	1.439	6.00	.270	.538	.104	28.21
70.4	.18388	1.456	3.99	.322	.707	.117	26.33
70.2	.28388	1.448	4.72	.304	.634	.110	26.88
70.1	.38388	1.440	5.61	.286	.568	.103	27.74
70.3	.48388	1.432	6.64	.269	.509	.096	28.63
80.4	.18388	1.449	4.43	.322	.668	.109	26.48
80.2	.28388	1.441	5.22	.303	.601	.103	27.18
80.1	.38388	1.434	6.13	.286	.541	.096	27.98
80.3	.48388	1.426	7.21	.269	.487	.089	29.22
90.4	.18388	1.443	4.84	.322	.638	.102	26.80
90.2	.28388	1.436	5.66	.303	.576	.096	27.50
90.1	.38388	1.429	6.60	.286	.520	.090	28.40
90.3	.48388	1.422	7.71	.269	.469	.084	29.63
100.4	.18388	1.438	5.21	.322	.614	.097	27.03
100.2	.28388	1.431	6.05	.303	.556	.091	27.73
100.1	.38388	1.424	7.03	.286	.503	.085	28.85
100.3	.48388	1.418	8.14	.269	.456	.080	30.03
110.4	.18388	1.434	5.54	.322	.594	.092	27.27
110.2	.28388	1.427	6.41	.303	.539	.086	28.11
110.1	.38388	1.421	7.41	.286	.490	.081	29.19
110.3	.48388	1.414	8.54	.269	.444	.076	30.45

Table 4

Properties Affecting Stability (Y = .38388, fixed)

Model	Z	$\Gamma_{1,c}$	$\varepsilon_c/10^5$	κ_c	κ_s	<s>	$\rho_c/<\rho>$
			(erg/gm sec)	(cm^2/gm)	(cm^2/gm)		
60.6	.01009	1.448	4.85	.289	.596	.108	25.85
60.1	.02009	1.447	5.00	.286	.604	.112	27.31
60.5	.04009	1.446	5.18	.282	.612	.116	30.28
70.6	.01009	1.441	5.44	.289	.561	.099	26.22
70.1	.02009	1.440	5.61	.286	.568	.103	27.74
70.5	.04009	1.438	5.81	.282	.575	.107	30.79
80.6	.01009	1.435	5.95	.288	.535	.093	26.50
80.1	.02009	1.434	6.13	.286	.541	.096	27.98
80.5	.04009	1.432	6.35	.281	.548	.100	31.21
90.6	.01009	1.430	6.41	.288	.514	.087	26.96
90.1	.02009	1.429	6.60	.286	.520	.090	28.40
90.5	.04009	1.427	6.83	.281	.526	.094	31.48
100.6	.01009	1.425	6.82	.288	.498	.082	27.30
100.1	.02009	1.424	7.03	.286	.503	.085	28.85
100.5	.04009	1.423	7.27	.281	.509	.089	31.98
110.6	.01009	1.421	7.18	.288	.485	.078	27.58
110.1	.02009	1.421	7.41	.286	.490	.081	29.19
110.5	.04009	1.419	7.66	.281	.494	.085	32.49

monotonic function of β, it exhibits similar behavior. Throughout most of the star Γ_1 is near or above 1.4. Thus the star is not in danger of dynamic instability.

At the high temperatures which exist near the center of the star, the opacity is almost entirely due to electron scattering. Pure Thomson scattering is, of course, a constant independent of temperature and density for a given composition. The actual opacity near the center is somewhat less than the Thomson-scattering value because of the change from Thomson to Compton scattering. Near the surface the contribution of bound-free absorption by metals is large enough that the opacity is nearly double the electron-scattering value. The central and surface values of opacity (κ_c and κ_s) are given in Tables 3 and 4. Note that if we consider opacity as a function of mass, all of the increase near the surface occurs in only the outer 1 percent of the mass. Thus opacity appears to be a nearly constant function of mass.

Almost all details of the static models agree very well with those of Shibata (1968). In addition, Shibata shows graphically many properties of upper-main-sequence stars which are useful in estimating the structure of such stars when quantitative accuracy is not necessary.

b) Linear Stability Analysis and Mass Limits

Each of the static models was analyzed by using the linear nonadiabatic method described in § II. To the best of our knowledge this is the first time a fully nonadiabatic analysis has been applied to this problem. The complex eigenfrequencies were found for the fundamental mode and the first two overtones. These eigenfrequencies are shown in Table 5 as periods in seconds and relative gains in kinetic energy per period.

The periods show no unusual or unexpected results. The fundamental periods range from approximately 6 to 10 hours and increase with mass and radius as expected. The values of $Q_0 = \Pi_0(\langle\rho\rangle/\langle\rho_\odot\rangle)^{1/2}$ for composition 1 range from $Q_0 = 0^d.064$ for 60 $\mathfrak{M}_\odot$ to $Q_0 = 0^d.088$ for 110 $\mathfrak{M}_\odot$. The periods of the first and second overtones are approximately one-half and one-third, respectively, of the fundamental period. Thus the small-amplitude oscillations are nearly harmonic.

The main results of the linear analysis are the relative gains in energy per period in the fundamental mode. These results are shown in Table 5 as $(\Delta E/E)_0$. A positive sign indicates instability; a negative sign, stability. In general we see that the fundamental mode becomes less stable as mass increases, as we expect. All of the first- and second-overtone modes are stable, with damping times approximately 10^{-3} and 10^{-4} of the fundamental damping time, respectively. The reason for this strong stability is that even for $\Gamma_1 = \frac{4}{3}$ the amplitudes of the overtone pulsations are small in the core where driving caused by nuclear reactions occurs. We also note that the overtones become more stable with increasing mass.

In order to find the maximum stable mass as a function of composition, the relative energy gains are plotted versus mass, and the zero point is found from the graph. These curves for all compositions are shown in Figure 2. Although there are some unexplained wobbles in a few of the curves, the mass limits seem to be determined at least to within ± 3 $\mathfrak{M}_\odot$. These maximum stable masses are given in Table 6 and shown on the (Y, Z)-plane in Figure 3.

These results show that as Y increases, for fixed Z, $\mathfrak{M}_c$ decreases monotonically. For fixed Y, $\mathfrak{M}_c$ decreases slowly with decreasing Z. Tables 3 and 4 show properties of the models which may aid in understanding these results.

First, we have tabulated Γ_1 at the stellar center. We see in both cases that $\Gamma_{1,c}$ is almost constant and independent of composition. Because the changes in $\Gamma_{1,c}$ are small we shall assume that, aside from being near enough to $\frac{4}{3}$ to allow pulsations to reach the stellar center, the exact value of Γ_1 is not an important factor in determining stability. Second, we might reasonably expect that higher central condensation will cause stabilization. Looking at $\rho_c/\langle\rho\rangle$ for the case of fixed Z, we see that the opposite seems to be

Table 5

Results of Linear Non-adiabatic Analysis

Model	Π_0 (sec)	$10^7\left(\frac{\Delta E}{E}\right)_0$	Π_1 (sec)	$10^4\left(\frac{\Delta E}{E}\right)_1$	Π_2 (sec)	$10^3\left(\frac{\Delta E}{E}\right)_2$
60.1	24179	- 6.51	12512	-2.43	9518	-2.69
70.1	26302	- 3.29	13234	-2.53	9680	-2.79
80.1	28262	+ 2.66	13859	-2.53	10134	-2.95
90.1	30098	+ 5.96	14444	-2.61	10559	-3.10
100.1	31832	+ 9.28	14998	-2.71	10961	-3.33
110.1	33474	+12.44	15500	-2.77	11327	-3.42
60.2	23291	- 6.59	12428	-1.93	9088	-2.09
70.2	25349	- 3.60	13096	-2.04	9572	-2.20
80.2	27273	- 1.76	13752	-2.16	10045	-2.34
90.2	29065	+ 0.71	14331	-2.24	10464	-2.43
100.2	30752	+ 3.81	14857	-2.25	10845	-2.44
110.2	32361	+ 6.49	15381	-2.30	11225	-2.53
60.3	25141	- 3.49	12645	-2.98	9264	-3.58
70.3	27305	+ 1.32	13326	-3.09	9761	-3.79
80.3	29321	+ 5.28	13982	-3.22	10239	-4.08
90.3	31204	+ 9.92	14563	-3.29	10662	-4.34
100.3	32975	+14.00	15085	-3.38	11042	-4.54
110.3	34661	+17.42	15606	-3.46	11422	-4.73
60.4	22448	- 8.23	12297	-1.66	8986	-1.73
70.4	24473	- 4.59	13011	-1.65	9501	-1.74
80.4	26339	- 2.06	13618	-1.73	9939	-1.83
90.4	28098	- 0.22	14214	-1.82	10371	-1.92
100.4	29753	+ 2.05	14756	-1.85	10761	-1.96
110.4	31321	+ 3.72	15246	-1.94	11116	-2.07
60.5	26111	-12.56	14071	-3.65	10293	-4.12
70.5	28377	- 8.33	14856	-3.96	10864	-4.50
80.5	30475	- 1.74	15559	-3.86	11376	-4.54
90.5	32432	+ 2.07	16182	-4.03	11830	-4.76
100.5	34293	+ 5.97	16812	-4.19	12287	-5.03
110.5	36055	+ 9.68	17387	-4.28	12705	-5.27
60.6	22602	- 3.18	11461	-1.83	8387	-2.09
70.6	25491	- 0.55	12122	-1.93	8866	-2.23
80.6	26427	+ 2.39	12691	-1.94	9276	-2.23
90.6	28154	+ 4.95	13248	-2.01	9679	-2.33
100.6	29779	+ 7.89	13752	-2.04	10045	-2.41
110.6	31317	+10.54	14211	-2.10	10378	-2.49

TABLE 6

MAXIMUM STABLE MASSES

Composition No.	Y	Z	$\mathfrak{M}_c/\mathfrak{M}_\odot$	$\mu^2\mathfrak{M}_c/\mathfrak{M}_\odot$
4.....	0.18388	0.02009	91.0	30.0
2.....	0.28388	0.02009	87.0	33.3
1.....	0.38388	0.02009	75.5	34.0
3.....	0.48388	0.02009	67.0	36.9
6.....	0.38388	0.01009	72.0	43.9
1.....	0.38388	0.02009	75.5	34.0
5.....	0.38388	0.04009	84.5	28.8

true. This is probably caused by the fact that the stabilizing effect of an increase in $\rho_c/\langle\rho\rangle$ is masked by changes in other physical variables as discussed below.

We look instead to the physical sources for driving and damping. Driving, as we have discussed, comes from the nuclear sources of energy. Damping, aside from a small contribution due to the temperature dependence of radiative flux, is caused by the negative temperature exponent of opacity. If we assume an opacity of the form $\kappa \propto V^{-n}T^{-s}$, then larger values of s imply larger damping. In Tables 3 and 4 we have tabulated a mean s for the star defined by

$$-\langle s\rangle = \frac{\log \kappa_c - \log \kappa_s}{\log T_c - \log T_e}. \tag{7}$$

This $\langle s\rangle$ will be a measure of the amount of damping in the envelope.

Looking first at the case of fixed Z (Table 3), we see that as Y increases, the central ϵ increases sharply and hence the amount of driving caused by nuclear sources increases.

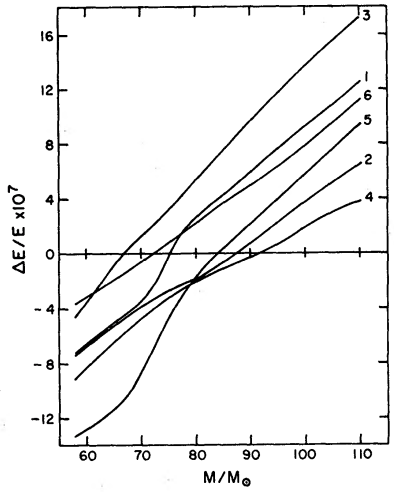

FIG. 2

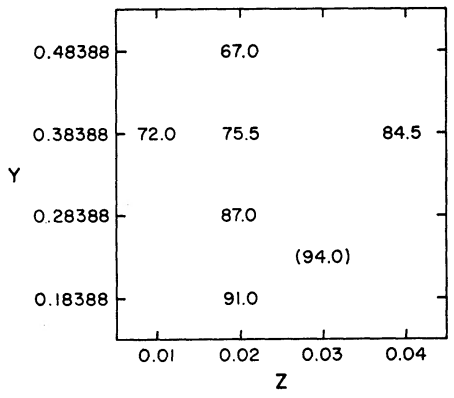

FIG. 3

FIG. 2.—Relative energy gain per period as a function of mass. Positive values indicate pulsational instability. The curve for each composition is labeled with the number given in Table 1.

FIG. 3.—Computed maximum stable masses shown at their respective points in the (Y, Z)-plane. The value in parentheses is the value given by the analytic fit for the Schwarzschild and Härm composition.

We also see that as Y increases, $\langle s\rangle$ decreases, so that the amount of damping decreases. Both of these effects lead to destabilization with increasing Y and thus to smaller values of $\mathfrak{M}_c$.

In the case of fixed Y the situation is less simple. From Table 4 we see that as Z increases, ϵ_c increases slowly, so driving is increased. Looking at $\langle s\rangle$, we see that as Z increases, $\langle s\rangle$ increases, so damping is increased. The result of the competition between these two effects, inferred after the fact from the results, appears to be that the effect of energy generation dominates.

The results of Stothers and Simon (1970) differ only slightly from these results. The reasons for these differences are not completely clear. There are, however, several points at which the methods of the two investigations differ. First, Stothers and Simon have used $X_{CNO} = \frac{1}{3}Z$ whereas we have used approximately 0.6 Z. Second, since they are mainly interested in the investigation of the effects of opacity, they have simplified the formula for energy generation so that the temperature dependence is always taken to be $\epsilon \propto T^{13}$. In our investigation we have used a more complete formula for energy

generation and find the minimum temperature exponent (at the stellar center) to be approximately 14. These differences between the two methods may well explain the differences in results.

We have constructed an analytic fit to our six values of $\mathfrak{M}_c$ as a function of composition. Unfortunately, since our composition points lie in two intersecting straight lines in the (Y, Z)-plane, our fit must have the form of a sum of functions of Y and Z alone with no cross-products. A least-squares fit to a plane in Y and Z gives

$$\mathfrak{M}_c = 100\ (1.00 + 4.19\ Z - 0.83\ Y) \pm 2.0\ . \tag{8}$$

We now compare our results with those of Schwarzschild and Härm (1959). For a composition with $X = 0.75$, $Y = 0.22$, and $Z = 0.03$, they found $\mathfrak{M}_c = 60\ \mathfrak{M}_\odot$. For this composition the value of $\mathfrak{M}_c$ given by equation (8) is $94\ \mathfrak{M}_\odot$, larger than the Schwarzschild and Härm value. This value is shown in parentheses in Figure 3. The main reason for this discrepancy seems clear. Schwarzschild and Härm assumed that opacity was purely Thomson electron scattering independent of ρ and T. But we have seen that the temperature dependence of opacity which occurs in the present models is an important damping mechanism. Thus if we ignore this effect, the star will appear more unstable and the computed critical mass will be too small.

Schwarzschild and Härm point out that if one assumed that stability is dependent only on Γ_1 which in turn is a monotonic function of β, one would predict that the composition dependence of $\mathfrak{M}_c$ should be such that $\mu^2\mathfrak{M}_c$ is constant. The last column of Table 6 shows this product, and it is nearly constant. The value of $\mu^2\mathfrak{M}_c$ from Schwarzschild and Härm is approximately 20, different from any of our results. It is not surprising that detailed calculations do not exactly confirm the simple prediction since, as we have seen, stability is a rather complicated combination of effects.

c) *Effects of the Amplification Factor*

In order to understand the qualitative nature of some of the physical effects of a large amplification factor, this factor was inserted into the linear nonadiabatic analysis. In this way the effects at small amplitude can be studied in some detail. Since we were interested in the effects of F on the dynamic evolution, the model used in these tests was Model 100.1, the model for which dynamic evolution was calculated.

One conclusion reached was that the argument given in § II concerning the mutual independence of momentum and energy time scales is valid over a very large range of values of nonadiabatic terms. In the case with $F \approx 4 \times 10^5$ so that $\Delta E/E = 1$, the nonadiabatic period differed from the adiabatic period by less than 2 percent.

The effects of F on the eigenfunctions are shown in the upper section of Figure 4. The radius and temperature eigenfunctions are exhibited in the following notation. We assume that

$$\frac{\delta r}{r} = \zeta e^{i\omega t}\ , \qquad \frac{\delta T}{T} = \tau e^{i\omega t}\ ,$$

where ζ and τ are complex spatial functions. We then write ζ and τ in the form

$$\zeta = |\zeta| e^{i\phi(\zeta)}\ , \qquad \tau = |\tau| e^{i\phi(\tau)}\ ,$$

where $|\zeta|$, $|\tau|$, $\phi(\zeta)$, and $\phi(\tau)$ are real functions which are plotted in Figure 3. Subscript 1 denotes the physically correct $F = 1$ solution. Subscript F denotes the solution with $F \approx 4 \times 10^5$. Normalization conditions have been applied which require $|\zeta| = 1$ and $\phi(\zeta) = 0$ at the surface.

We see that the amplitudes are not qualitatively changed by the amplification factor. They are, however, systematically lowered by approximately 30 percent. The phases are qualitatively changed by the presence of the amplification factor. In the physical

case the phases are nearly constant and are π out of phase with each other. With the amplification factor present, the phases increase markedly as one goes inward. The phase difference of π between ζ and τ is approximately maintained except in the nuclear-generation region.

The lower section of Figure 4 shows the effect of F on driving and damping. We consider individual mass zones in the star as separate heat engines and compute the amount of work done per zone during one period. If the work is positive, the zone is driving; if negative, the zone is damping. The total change in energy per period of the star is the

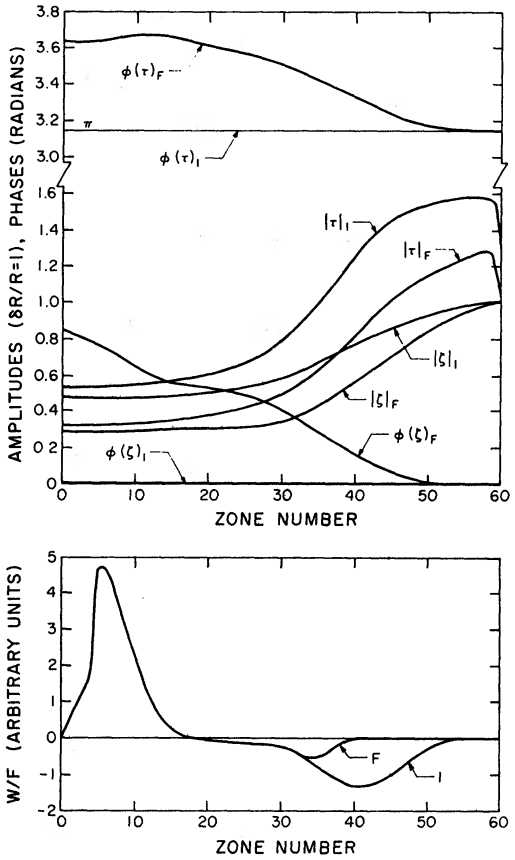

FIG. 4.—Small-amplitude effects of the amplification factor. Upper section shows the amplitudes and phases of the radius and temperature eigenfunctions. Lower section shows the relative energy gain per period of each zone. In all cases subscript 1 indicates no amplification factor and subscript F indicates $F = 4.123 \times 10^5$.

sum of the changes for all zones. We have plotted the work done by each zone W divided by the amplification factor F. The labeling of the curves is the same as in the upper section of Figure 4.

In the physical case we see exactly what we expect. Near the center where nuclear generation of energy occurs there is a strong driving region. Outside the driving region there is an intermediate region containing a large part of the stellar mass in which there is a small amount of damping. This is the region in which the opacity is still mainly electron scattering and nearly constant. Thus this small damping is that caused by the temperature dependence of the equation of radiative transfer mentioned in the previous section. Finally, in a zone near the surface containing only a small amount of mass, we see a larger damping contribution. This is damping caused by the temperature depen-

dence of opacity. The net area under the curve is the total energy gain over a period of the star.

If the effect of the amplification factor were linear and uniform through the star, we should expect that when we divide W by F we would recover the same curve as for $F = 1$. We see that this is true except for a region near the surface in which the damping is reduced relative to driving when F is inserted. The explanation of this effect is the following.

Near the surface of every star there is a region which Cox and Giuli (1968) call the transition region. This region is defined as the region in which the nonadiabatic term in the energy equation becomes comparable with the adiabatic term. Outside the outer boundary of this region the nonadiabatic term dominates, and the energy equation (e.g., eq. [3]) becomes (if one assumes $\epsilon = 0$ near the surface)

$$\frac{\partial L_r}{\partial \mathfrak{M}_r} = 0 . \tag{9}$$

Thus outside the transition region L_r is constant in space at all times. Therefore, at the instant of maximum compression, zones outside the transition region are neither driving nor damping. A much more complete description of the transition region and its important effects on stellar stability is given in chapter 27 of Cox and Giuli (1968). Since the reason for introducing the amplification factor F is to increase the size of the nonadiabatic term relative to the adiabatic term in the energy equation, its effect is clearly to move the transition region inward. Thus more of the damping region will be removed but the driving region will be unaffected, as shown in Figure 4.

d) Dynamic Evolution

We shall now discuss the dynamic results. An amplification factor $F = 4.123 \times 10^5$ was used to make $\Delta E/E = 1$. Even so, since the Courant condition which limits possible time steps is determined in the core where temperatures are high, each period required from 500 to 1000 time steps and from 6 to 10 minutes of computing time. Thus we wished to start the calculation at a finite amplitude and to reduce unwanted transients as much as possible. This was done by using the linear nonadiabatic results including F to compute an input perturbation. The relative phases of all variables were carefully taken into account so that the pulsation was initiated in the fundamental mode with a minimum of transients. The size of the perturbation was fixed by requiring $\delta r/r = 0.1$ at the surface.

The results showed that except for some small transient noise near the surface, the initiation of the fundamental mode was highly accurate. The period was equal to the linear period as closely as could be determined. The growth rate was such that the ratio of kinetic energies at maxima one period apart was 2.5, nearly the factor e expected if $\Delta E/E = 1$.

With the amplification factor multiplying the nonadiabatic term we must be careful in our definitions of time when looking at the results. Recall that the effect of F is to shorten the time scale for changes in energy relative to that for changes in momentum. The time variable used in the computation is the momentum time, t_{mom}, and all graphs are plotted with t_{mom} used as the independent variable. For phenomena related to energy changes we must always convert to the energy time, t_{en}, by using the relation $t_{\text{en}} = F t_{\text{mom}}$.

In Figure 5 we show a computer-generated plot of the radii of all sixty mass shells in the star as a function of time. The topmost curve represents the surface of the star. We see that in the central regions the radii pulsate about approximately constant equilibrium values until a limiting amplitude is reached. The outer zones begin to oscillate symmetrically about equilibrium values with some noise caused by the finite perturbation discussed above. As nonlinear effects become important, the inward excursions

become much smaller than outward excursions. The result of this nonsymmetric oscillation is an increase in the mean radius of the star. Although these outer zones did not reach a steady periodic motion before the calculation was ended, these zones contain so little mass that they make very little contribution to the total kinetic energy of the star. In terms of this kinetic energy a limiting amplitude is reached at $t_{\text{mom}} \approx 4 \times 10^5$ seconds or $t_{\text{en}} \approx 1.6 \times 10^{11}$ seconds.

Slightly before this limiting amplitude is reached the envelope expands to approximately 4 times its equilibrium radius. As this envelope contracts, the star develops some characteristics of first-overtone pulsation. A clearly defined node develops near the surface. Some indication that this is indeed a first-overtone pulsation is given by the following order-of-magnitude argument. We assume that the first overtone obeys the period–mean density relation and that when the surface reaches periodic, limiting-amplitude oscillation it will have a mean radius approximately twice the equilibrium

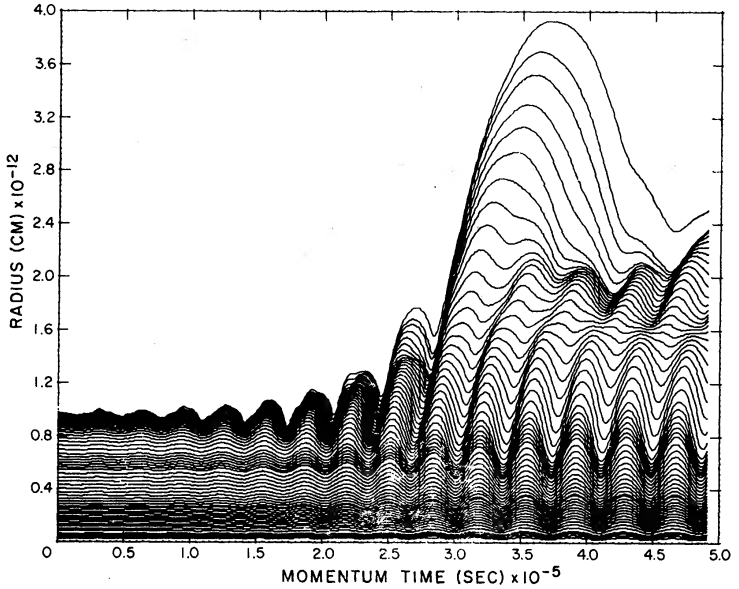

FIG. 5.—Computer plot of the radii of all zones versus momentum time. *Topmost curve*, surface of the star.

radius. Then the first overtone period should be approximately $2^{3/2}$ times the first-overtone period obtained in the linear calculation, or 4.2×10^4 seconds. After limiting amplitude is reached, the dynamic period is approximately 3.8×10^4 seconds. This near agreement lends some credibility to our interpretation. The appearance of the node at approximately 80 percent of the assumed mean radius is also typical for a first-overtone pulsation.

Temperature and pressure are qualitatively similar to one another. Except near the surface, the oscillations are nearly symmetric and grow to a limiting amplitude. The only unusual behavior is the almost complete lack of evidence for the first-overtone pulsation. In the temperature no node appears. In the pressure there is some behavior similar to a node, but phases on either side of this node are not those characteristic of a first overtone. The detailed explanations of these behaviors are not clear.

In Figure 6 are plotted the surface velocity (positive outward) and total luminosity versus time. The velocity shows clearly the transient noise at early times since velocity itself is a perturbation quantity. The oscillation then becomes very asymmetric. The long times when velocity is positive compared with shorter times when velocity is negative reflect the increase of mean radius. At the time when velocity reaches its maximum

outward value of 5×10^7 cm sec^{-1}, the escape velocity is 12×10^7 cm sec^{-1}. At the instant of maximum radius the escape velocity has its minimum value, 8.2×10^7 cm sec^{-1}, but the surface velocity at this time is of course zero.

The luminosity amplitude grows smoothly to the limiting value, about 1 mag. None of the peculiarities of other surface variables show up in the luminosity. This is probably caused by the fact that, as discussed above, the luminosity is constant in space down to the transition region, which lies below the node.

The major finding from our dynamic calculation is that limiting amplitude is reached without mass loss. Since this limiting amplitude is reached after approximately 10^{11} seconds and the nuclear time scale for 100 $\mathfrak{M}_\odot$ is approximately 10^{13} seconds, stabilization by nuclear evolution cannot account for the absence of mass loss. Two possible explanations for the existence of the limiting amplitude are discussed below. It seems likely that, because of our use of the amplification factor, the cause may be different for the calculation than for a real star.

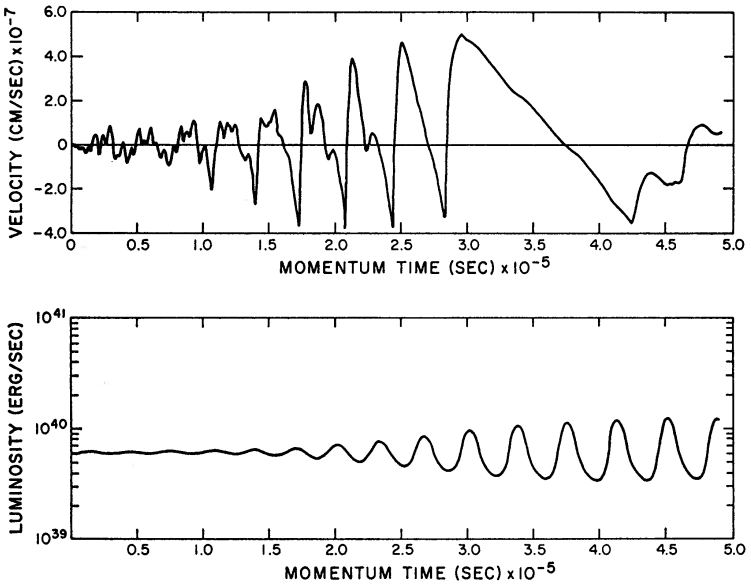

FIG. 6.—Computer plots of surface velocity and total luminosity versus momentum time

The first possible explanation is the mixture of the first overtone into the pulsation. Since the first overtone is very stable in the linear analysis, only a small mixture of this mode would be necessary to stabilize the pulsations at small amplitudes. The problem of large-amplitude stability for overtones has not been solved in this investigation. Neither has the effect of F on the overtones been investigated. Thus we cannot say for certain that a mixture of fundamental and first overtone would be more stable than the fundamental alone. Although this explanation may account for the limiting amplitude in the calculation, it appears that in the physical case the limiting amplitude may be much smaller because of the mechanism suggested in the second possible explanation, i.e., shock-wave dissipation.

As nonlinear effects become important in the dynamic calculation, shock waves form near the stellar surface. These waves form approximately at the time of minimum radius and reach the surface during the expansion phase a short time after minimum radius. The effect of these shock waves is to convert the directed kinetic energy into internal energy. The method used to handle shocks in our calculation was the well-known artificial-viscosity method (Richtmyer and Morton 1967). The specific form used follows Cox *et al.* (1966). In principle, the artificial viscosity smooths the shock waves but does

not change the energy dissipated by them. A rough estimate of the amount of shock-energy dissipation during the one period immediately preceding the large envelope expansion and attainment of limiting amplitude shows that about 10^{44} ergs were dissipated. Since the maximum kinetic energy during that period was 10^{49} ergs, it appears at first sight that shock dissipation is not important. We must, however, point out that shock-wave dissipation is an outstanding exception to the separation of energy and momentum time scales. Since shock waves appear every period, they are a momentum phenomenon. But shock waves dissipate energy and in that sense are an energy phenomenon. The result is that when we use the amplification factor to reduce the number of periods in a growth time from 10^6 to 1, we underestimate the shock-energy dissipation by a similarly large factor. Thus, although shock dissipation in the present calculation seems unimportant, in the physical case it may well be the dominant mechanism of dissipation. If this is true, the limiting amplitude may well be much smaller than we have calculated. We may, in fact, have found an upper limit to possible limiting amplitudes for the kind of stars under investigation.

By shock-energy dissipation we of course mean that the directed energy of the shock wave is converted to random thermal energy. Since this occurs in the outer layers of the star which contain only a very small fraction of the stellar mass, the effect of this large amount of thermal energy may be considerable. The solution of this problem would require a much more detailed consideration of the shock-wave phenomena and has not been attempted. The actual problem of massive main-sequence stars, however, must include such detailed consideration.

IV. SUMMARY AND CONCLUSIONS

Two main conclusions arise from this investigation. First, the maximum stable mass is not a very sensitive function of composition. Second, mass loss may not occur even for stars well above the maximum stable mass. The implications of these conclusions will be discussed separately.

From the composition dependence of the mass-stability limit we can state that for a random collection of stars there is no single upper limit associated with pulsational instability. There is instead a range of masses which may or may not be unstable, depending on composition. This range may extend from approximately 10 $\mathfrak{M}_\odot$ for pure-helium stars to 200 $\mathfrak{M}_\odot$ for pure-hydrogen stars (if enough heavy elements are assumed so the CNO cycle operates). In a cluster where we have reason to suspect that all stars have the same composition there will be a definite upper mass limit. Since the nuclear evolution time for stars above this limit is approximately 10^5–10^6 years, only in extremely young clusters would we expect to see main-sequence stars with masses above the limit.

The conclusions to be drawn from the dynamic case are much less clear. If we accept the result that a limiting amplitude will be reached before mass loss occurs, then the hypothesis that there exists an upper limit to stellar masses is not confirmed. Instead, we must say that above a certain mass homogeneous stars are pulsationally unstable, grow to a limiting amplitude, and then later are stabilized by nuclear evolution. This evolutionary stabilization and the theoretical and observational implications of the conclusions suggested by this investigation are discussed by Stothers and Simon (1968).

The result of Osaki (1966), who found that stars of 10^4–10^5 $\mathfrak{M}_\odot$ will lose enough mass to reach the stability limit of about 100 $\mathfrak{M}_\odot$ cannot be checked by this investigation. The fact that Osaki did not consider shock dissipation at any point in his calculations means, however, that he may have neglected the most important cause of a limiting amplitude.

The observational problem at the upper end of the main sequence is very difficult. The bolometric correction increases with temperature nearly as fast as the luminosity. Thus the visual magnitude of stars at the upper end of the main sequence is nearly independent

of their mass and luminosity. In addition, the very sharp decrease in the relative numbers of stars with increasing mass makes observation of large-mass stars unlikely. If the true limiting amplitude is smaller than that calculated in this investigation, this may account in part for the lack of observed variations in upper-main-sequence stars. In addition, it has been pointed out by Simon and Stothers (1970) that a star with high surface temperature and high radiation pressure may pulsate at large amplitude but not show large light variations in the usual U, B, V colors. A recent paper by Morton (1969) gives new values for temperatures and bolometric corrections for O stars. This work, in addition to observations made from above the atmosphere, may clarify the observational problem.

As a final summary of the results we may say that the effect of radiation pressure in causing an upper mass limit to pulsationally stable homogeneous stars is not very sensitive to composition. We may say with less certainty that because of shock-wave dissipation this instability probably does not cause a maximum stellar mass but only a short phase characterized by pulsation before nuclear evolution stabilizes the star. If this conclusion is correct, stars whose masses are above the pulsational stability limit on the main sequence may exist in apparently normal post–main-sequence states.

It is a pleasure to thank John P. Cox for suggesting this problem and providing the continuing advice and encouragement necessary for its completion. For help in computing techniques and providing some of the computer programs used as well as valuable physical insights the author would like especially to thank John Castor, Carl Hansen, and Bodhan Paczyński.

This work was supported in part by NSF grant GP-12455 through the University of Colorado and in part by NASA and NSF through Predoctoral Traineeships.

REFERENCES

Aller, L. H. 1961, *Abundances of the Elements* (New York: Interscience Publishers).
Appenzeller, I. 1970, *Astr. and Ap.*, **5**, 355.
Boury, A., Gabriel, M., and Ledoux, P. 1964, *Ann. d'ap.*, **27**, 92.
Castor, J. I. 1970 (in preparation).
Cox, A. N., Brownlee, R. R., and Eilers, D. D. 1966, *Ap. J.*, **144**, 1024.
Cox, J. P., and Giuli, R. T. 1968, *Principles of Stellar Structure* (New York: Gordon & Breach).
Cox, A. N., and Stewart, J. N. 1965, *Ap. J. Suppl.*, **11**, 22.
Fowler, W. A., Caughlan, G. R., and Zimmerman, B. A. 1967, *Ann. Rev. Astr. and Ap.*, **5**, 525.
Henyey, L. G., Wilets, L., Böhm, K. H., LeLevier, R., and Levée, R. D. 1959, *Ap. J.*, **129**, 628.
Ledoux, P. 1941, *Ap. J.*, **94**, 537.
Morton, D. C. 1969, *Ap. J.*, **158**, 629.
Osaki, Y. 1966, *Pub. Astr. Soc. Japan*, **18**, 384.
Paczyński, B. 1969 (personal communication).
Richtmyer, R. D., and Morton, K. W. 1967, *Difference Methods for Initial Value Problems* (2d ed.; New York: Interscience Publishers), pp. 262 and 313.
Schwarzschild, M., and Härm, R. 1959, *Ap. J.*, **129**, 637.
Shibata, Y. 1968, *Sci. Rept. Tôhoku Univ.*, First Ser., **51**, 95.
Simon, N. R., and Stothers, R. 1970, *Astr. and Ap.*, **6**, 183.
Stothers, R., and Simon, N. R. 1968, *Ap. J.*, **152**, 233.
———. 1970, *ibid.*, **160**, 1019.
Talbot, R. J. 1970 (in preparation).
Ziebarth, K. 1970, *Bull. A.A.S.*, **2**, 227.